# Characterization and *in vivo* evaluation of chitosan-hydroxyapatite bone scaffolds made by one step coprecipitation method

**Sergei N. Danilchenko,[1] Oksana V. Kalinkevich,[1] Maksim V. Pogorelov,[2] Aleksei N. Kalinkevich,[1] Anatoly M. Sklyar,[3] Tatyana G. Kalinichenko,[1] Vyacheslav Y. Ilyashenko,[1] Vadim V. Starikov,[4] Valentina I. Bumeyster,[2] Vitaly Z. Sikora,[2] Leonid F. Sukhodub[1]**

[1]Institute for Applied Physics, Department of Biophysics, National Academy of Sciences of Ukraine, Petropavlovskaya St. 58, Sumy, Ukraine
[2]Sumy State University, Medical Institute, Department of Human Anatomy, Sanatornaya St. 31, Sumy, Ukraine
[3]Sumy State Pedagogical University, Department of Chemistry, Romenskaya St. 87, Sumy, Ukraine
[4]National Technical University "Kharkov Polytechnic Institute", Department of Metal Physics, Frunze St. 21, Kharkov, Ukraine

Received 26 June 2009; revised 16 September 2010; accepted 18 November 2010
Published online 25 January 2011 in Wiley Online Library (wileyonlinelibrary.com). DOI: 10.1002/jbm.a.33017

**Abstract:** Chitosan/hydroxyapatite scaffolds could be used for bone regeneration in case the application of auto- or allografts is impossible. The objective of the present work was to characterize and study *in vivo* biodegradation of simple chitosan/hydroxyapatite scaffolds. For this purpose, a series of chitosan/hydroxyapatite composites has been synthesized in aqueous medium from chitosan solution and soluble precursor salts by a one step coprecipitation method. A study of *in vivo* behavior of the materials was then performed using model linear rats. Cylindrical-shaped rods made of the chitosan/hydroxyapatite composite material were implanted into tibial bones of the rats. After 5, 10, 15, and 24 days of implantation, histological and histo-morphometric analyses of decalcified specimens were performed to evaluate the stages of biodegradation processes. Calcified specimens were examined by scanning electron microscopy with X-ray microanalysis to compare elemental composition and morphological characteristics of the implant and the bone during integration. Porous chitosan/hydroxyapatite scaffolds have shown osteoconductive properties and have been replaced in the *in vivo* experiments by newly formed bone tissue. © 2011 Wiley Periodicals, Inc. J Biomed Mater Res Part A: 96A: 639–647, 2011.

**Key Words:** chitosan, hydroxyapatite, scaffolds, biodegradation, osteogenesis

## INTRODUCTION

Composites comprising calcium phosphates and natural biopolymers are widely used as biomaterials for bone tissue repair and engineering.[1–5] Hydroxyapatite, $Ca_{10}(PO_4)_6(OH)_2$, has been used as a principal inorganic component of synthetic materials for orthopaedy and stomatology for a long time. This mineral can be regarded, with some limitations, as a crystallochemical analog of the main mineral constituent of human and animal skeletal tissues.[6] A wide range of biomaterials for different clinical applications can be created on the basis of two components: nanocrystalline apatite and chitosan.[3–5,7–22] Chitin is the second (after cellulose) most abundant natural polysaccharide. It forms the skeletal system of arthropoda, it is also present in cell walls of fungi and bacteria. The hardness of chitin skeletal structures of arthropoda is caused by the formation of natural chitin-calcium carbonate-protein complexes. Chitosan is a derivative of chitin, which can be obtained by chitin deacetylation. Chitin and chitosan are polymorphous uncrystalline or partly crystalline biopolymers. Both of them contain same monomers, *N*-acetyl-2-amino-2-deoxy-D-glucopyranose and 2-amino-2-deoxy-D-glucopyranose, differing in the proportion of acetylated and deacetylated monomers. Chitin and chitosan are promising materials for medical applications due to their bacteriostatic/bactericide properties, biocompatibility with human tissues, and ability to facilitate regenerative processes in wound healing.[17,23] In recent years, the interest in chitosan/hydroxyapatite composite biomaterials increases significantly, which is expressed in a great number of scientific articles related to their characterization and tests. There are several ways to produce such composite materials. Most of them involve two major stages: first, the synthesis of an organic polymeric scaffold of pure or chemically treated and modified chitosan and, second, mineralization of the scaffold in simulated body fluid (the biomimetic way) or in saturated matrix solutions.[7–20] The scaffolds can be made in the form of membranes, microspheres,[24] or multilayered materials. Chitosan in such polymer substrates for mineralization can be combined with other macromolecules, such as silk fibroin or carboxymethylcellulose.[11,14] Also chitin can be used as a scaffold.[13,22] An inverse approach has also been described: the pre-formation of a porous hydroxyapatite scaffold with the consequent impregnation of it by chitosan.[8] The composites obtained in such ways were characterized by different physico-chemical methods to test their potential as biomaterials, and also a

**Correspondence to:** A. N. Kalinkevich; e-mail: kalinkevich@gmail.com

**TABLE I. Chitosan-to-Apatite Ratio of Samples Estimated from Thermogravimetric Measurements**

| | Ch/Ap preparation | | | Data of thermogravimetric analysis | | |
|---|---|---|---|---|---|---|
| | | Mineral solution | | Percentage of components determined from the weight loss | | |
| No | Ch/Ap composites, (specified weight ratio) | $CaCl_2$ 1*M*, mL | $NaH_2PO_4$ 1*M*, mL | $H_2O$, wt % | Chitosan, wt % | Apatite, wt % |
| 1 | ChAp 15/85 | 113.3 | 68.0 | 9.0 ± 1.2 | 14.9 ± 3.09 | 76.1 ± 3.09 |
| 2 | ChAp 30/70 | 46.6 | 28.0 | 11.4 ± 0.2 | 25.4 ± 0.60 | 63.2 ± 0.60 |
| 3 | ChAp 50/50 | 20.0 | 12.0 | 3.3 ± 1.0 | 49.3 ± 2.2 | 47.4 ± 2.2 |
| 4 | ChAp 80/20 | 5.0 | 3.0 | 8.9 ± 1.0 | 73.0 ± 2.0 | 18.1 ± 2.1 |

In each case 1000 mL of 0.2 wt % chitosan solution was used for Ch/Ap preparation.

series of biocompatibility tests using cell cultures were performed, confirming biocompatibility of these composites.[8–14] In addition, some researchers have reported one-step schemes of chitosan-hydroxyapatite synthesis. Yamaguchi et al.[3] have described a one step approach, in which the composite was coprecipitated by dropping chitosan solution containing phosphoric acid into calcium hydroxide suspension. Rusu et al. have developed a stepwise coprecipitation approach using it to obtain different types of chitosan/hydroxyapatite composites with different ratios between their components.[4] These composite materials have also been thoroughly characterized by physico-chemical techniques and have found to contain nanosized hydroxyapatite with structural features close to those of biological apatites. A further development of this approach was proposed by Chesnutt et al., they have developed microsphere-based chitosan/nanocrystalline calcium phosphate composite scaffolds.[25] It seems that a combination of physico-chemical and structural characterization of biomaterials with their preclinical *in vivo* investigations is necessary to find out how the changes in structure and composition of the investigated biomaterials affect their behavior in living organisms. Since chitosan/hydroxyapatite materials could be used in bone regeneration as scaffolds in case the application of auto- or allografts is impossible for some reasons, investigation of biodegradation processes *in vivo* is important for further progress in this area (as long as an ideal scaffold material is not yet available). In the present work we have tried to synthesize, characterize and evaluate *in vivo* behaviour of the simplest (uniform, made by a one-step technique) chitosan/hydroxyapatite materials as a first step towards the *in vivo* investigation of more complicated scaffold systems.

## MATERIALS AND METHODS

### Materials preparation and characterization

The examined series consists of materials with different chitosan/apatite concentration ratios. The low molecular weight chitosan from Sigma-Aldrich (degree of deacetylation 75–85%; Brookfield viscosity 20–200 cP) was used. The substances were obtained by adding aqueous solutions of $CaCl_2$ and $NaH_2PO_4$ (keeping Ca/P ratio equal to 1.67) into 0.2% solution of chitosan in 1% acetic acid. The necessary pH level was maintained by adding NaOH. The details of the sample preparation are listed in the Table I. Products of the synthesis were aged, rinsed thoroughly, and then dried. Water content and chitosan-to-apatite ratio were estimated by weighing the samples before and after annealing in air at the temperature of 130°C and 900°C for 45 min.

To obtain porous materials, a lyophilization procedure was applied to wet (not dried completely) substances by using the vacuum chamber VUP-5M (SELMI, Ukraine) in which a glass sample-holder cooled with liquid nitrogen had been mounted. The frozen samples were dried under $10^{-3}$ Pa overnight.

Infrared spectra were measured on the Spectrum One spectrometer (Perkin Elmer). Before examination the powdered samples were mixed with KBr powder (2.5–3.0 mg of chitosan/apatite composite and 300 mg of KBr) and pressed into a solid disk. The Vickers hardness of the non-porous samples was measured by the standard method using the special light microscope PMT-3 (LOMO, Russia). The load of 20 grams was applied to each sample.

X-ray diffraction (XRD) crystallographic investigations were performed using the diffractometer DRON4-07 ("Burevestnik", Russia). The Ni-filtered CuK$\alpha$ radiation (wavelength 0.154 nm) was used with a conventional Bragg-Brentano geometry $\vartheta$-$2\vartheta$ (where $2\vartheta$ is the Bragg's angle). The current and the voltage of the X-ray tube were 20 mA and 30 kV, respectively. The samples were measured in the continuous registration mode (at the speed of 2°/min) within the $2\vartheta$-angle range from 8 to 60°. All experimental data processing procedures were performed with the program package DIFWIN-1, ("Etalon PTC" Ltd.).

Scanning electron microscopy with X-ray microanalysis was performed using the electron microscope REMMA102 (SELMI, Ukraine). This instrument allows visualization of sample surface with the limit resolution of ca. 10 nm. Characteristic X-ray emission exited by the electron probe makes it possible to estimate the elemental composition of a sample. In this work the accelerating voltage of the electron probe was set to 20 kV, the current of the probe was set to 2 nA. An energy dispersive X-ray (EDX) detector was used. The analytical signal of characteristic X-ray emission was integrated by scanning the $50 \times 50$ $\mu m^2$ area of sample surface.

To avoid surface charge accumulation in the electron-probe experiment, samples were covered with the thin (30–50 nm) layer of silver in the vacuum set-up VUP-5M (SELMI, Ukraine).

### Animal tests

For the *in vivo* tests 48 linear laboratory rats at the age of 4 months were used. The Ukrainian National Act of animal protection against cruel treatment (Act No 3447-IV 21.02.2006) regulating the care and use of laboratory animals has been observed. At the middle one-third of right tibia of the animals perforated defects were made with a stomatological borer, diameter 2 mm, in the sterile operating room. The width of a tibial diaphysis of adult rats is at the average from 4.2 to 4.7 mm. When a perforating bone defect is modeled, it is necessary to preserve integrity of bone, which causes the intramembranous type of bone regeneration. A model defect in this case cannot be wider than 2 mm. The 50/50 chitosan-hydroxyapatite scaffolds were chosen for *in vivo* evaluation. In the experimental group of animals cylindrical ChAp rods were implanted into traumas, diameter of the rods was equal to the width of the wound channel. The control group was comprised of the rats with the analogous tibial defects, which were not filled with the investigated material. The animals were taken out of the experiment after 5, 10, 15, and 24 days after implantation. The terms of taking out corresponded to the main stages of reparative osteogenesis.[26] The extracted bones with the defects were fixed in 10% formalin and then embedded in paraffin to prepare histological specimens. Some bones were treated with glutaraldehyde for the electron microscopy. The histological and histomorphological analyses of the extracted tissues were performed at the above mentioned stages of reparative bone regeneration.

### Characterization of specimens after the *in vivo* tests

Elemental composition and morphologic characteristics of the tissues were studied by scanning electron microscopy with the X-ray microanalysis. At the same time the blood samples were taken from the caudal vein for the biochemical analysis. The levels of calcium in serum, alkaline phosphatase and crude protein were examined. The crude protein in blood plasma was estimated by Lowry method. The calcium content in blood plasma was examined using the murexide-glycerin reagent. The alkaline phosphatase activity was determined by decomposition of phenylphosphate with the formation of phenol and consequent reaction of the phenol with 4-aminophenazone.

To prepare histological specimens the places of defects were extracted, fixed in 10% solution of neutral formalin, decalcified in EDTA solution during two months, dehydrated in alcohol solutions with increasing alcohol concentrations, and finally embedded in paraffin. Histological microscopic sections 10–12 μm thick were prepared and stained with azure-eosine and by van Giezon.[27] The microscopic sections were then investigated using an "Olimpus" light microscope with a digital camera.

Morphometry study has been carried out using the specialized computer programs "VideoTest 5.0" and "VideoSize 5.0" (St. Petersburg, Russia). Five days after the defects were made, the cellular composition of regenerated tissue was investigated, that is, the percentage of certain cell populations compared with the total amount of cells in the place of a defect. The number of fibroblasts, macrophages, lymphocytes, plasmocytes, neutrophils, and undifferentiated cells was calculated. Cells in the samples were counted under 1000× magnification, which allows to determine the phenotypic peculiarities of different cellular populations. Poorly differentiated bone marrow cells and undifferentiated connective tissue cellular elements were defined as undifferentiated cells. The cells had been counted over the whole section of a model defect. The number of macrophages, lymphocytes, fibroblasts, plasmocytes, and undifferentiated cells is given as percentage to the total number of cells in the defect. In histological specimens of the next stages of reparative osteogenesis the percentage of granulation, fibroreticular, membrane reticulated, splenial bone tissues as well as of red bone marrow were determined.

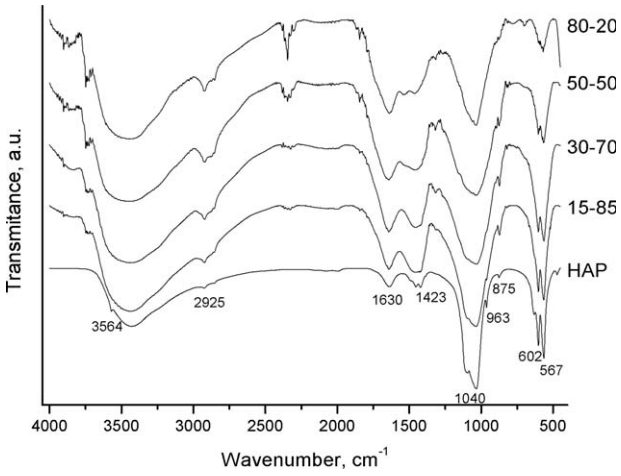


**FIGURE 1.** IR spectra of hydroxyapatite and chitosan/hydroxyapatite scaffolds with different chitosan/hydroxyapatite ratio.

## RESULTS AND DISCUSSION

The preparation conditions for series of ChAp composites and their chitosan-to-apatite ratio estimated by simple thermogravimetric analysis are listed in the Table I. The water content was estimated from the weight loss after heating the samples at 130°C. The total mineral (calcium phosphate) content was measured as a sample weight after complete burnout of organic moiety at 900°C. Here we assume, that the weight loss at 130°C corresponds to the water fraction and the weight loss at 900°C corresponds to the polysaccharide fraction.[3] As it is seen, the experimental data are in reasonable agreement with the declared chitosan-to-apatite ratio.

From IR spectroscopy studies of ChAp series with different proportions between components we can conclude that the major absorbance bands of IR spectra correspond to hydroxyapatite, though their width increases significantly and the bands characteristic to chitosan appear as the chitosan content increases (Fig. 1). The bands at 1000–1100 $cm^{-1}$ and 500–600 $cm^{-1}$ correspond to different modes of $PO_4$ group in hydroxyapatite.[28] Broadening of the band at 1050 $cm^{-1}$ reflects the presence of polymer and its interaction with phosphate groups.[20] The bands at 1420–1485 $cm^{-1}$ and at

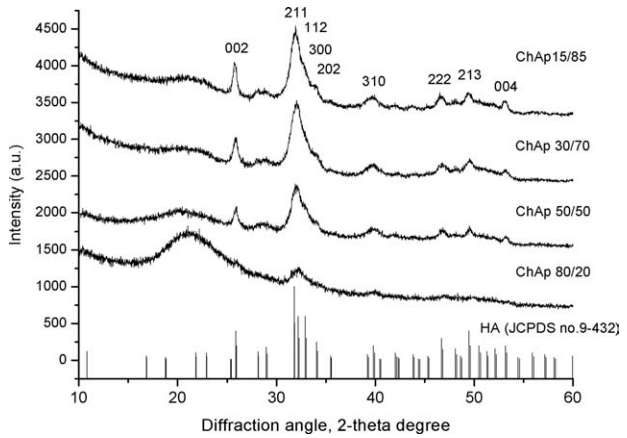


**FIGURE 2.** X-ray diffraction patterns of ChAp samples with different initial component ratio; the lines marked with Miller indices belong to hydroxyapatite. At the bottom there is a theoretical pattern of hydroxyapatite according to JCPDS.

$\sim$875 $cm^{-1}$ are derived from carbonate ions in apatite.[29] The phosphate stretching vibration bands from hydroxyapatite were indicated at 1000–1100 $cm^{-1}$ whereas the phosphate bending vibration bands situated at 500–600 $cm^{-1}$. The strongest characteristic $CO_3$ bands at 1420–1485 $cm^{-1}$ are also visible. The bands at 1550–1700 $cm^{-1}$ can be attributed to superposition of hydroxyapatite OH group and chitosan amide I and amide II. The bands at 3600–3700 $cm^{-1}$ can be assigned to hydroxyl groups present in the structure of chitosan,[14] the bands at 2800–2950 $cm^{-1}$ belong most probably to C—H stretch.[30,31]

XRD patterns suggest the presence of nanocrystalline apatite, its crystallinity decreases as content of chitosan increases (Fig. 2). As it follows from the diffraction peak broadening, which is inversely proportional to the crystallite size, the more chitosan is present in the composite, the less is the average size of apatite crystals. The semiquantative evaluation of the crystallite size were performed by the analysis of (002) line profile in the same way as in the work.[32] Shortly, at the negligible lattice microstrain, the crystallite size was determined from the physical broadening of the (002) line from Scherrer's formula:[33]

$$L = \frac{K\lambda}{\beta \cdot \cos\vartheta}$$

where $\beta$ is the line breadth of the pure diffraction profile resulting from small crystallite size, and $K$ is a constant approximately equal to unity and related to crystallite shape. Powdered polycrystalline NaCl was used as reference material free of size and microstrain broadening. The result of estimation suggests that for chitosan/apatite ratio equal to 50/50, the size of apatite crystallites in the composite is $\sim$20 nm, which is comparable with the crystallite size of bioapatite in bone tissue. The average size of bone apatite is normally $\sim$20 nm, which was proved by different experimental techniques.[34,35] Slightly increased intensity of the (002) and (004) peaks compared with the reference data suggests that the apatite crystallites are elongated along the crystallographic axis **c** (what is also characteristic for bioapatite of bone tissue). The XRD analysis in combination with IR spectroscopy studies clearly indicated the formation of chitosan/hydroxyapatite composites.

**TABLE II. The Vickers Hardness of the Samples with Different Chitosan-to-Apatite Ratio**

| No | Ch/Ap composites, (specified weight ratio) | Vickers hardness, GPa |
|---|---|---|
| 1 | ChAp 15/85 | 0.22 |
| 2 | ChAp 30/70 | 0.15 |
| 3 | ChAp 50/50 | 0.12 |
| 4 | ChAp 80/20 | 0.14 |

The Vickers hardness of nonporous ChAp composites is shown in the Table II. These data indicate the decrease of material strength with the increase of chitosan percentage and are in reasonable agreement with the value of 0.396 GPa recently reported for the cortical bone.[36] The porous composite materials are much less hard than the solid ones; their measured hardness values were too much spread to be conclusive; it was difficult to measure the dent size because of the complicated profile of sample surface.

Ca/P ratio in the ChAp samples measured by scanning electron microscopy with EDX microanalysis was close to that of apatite (1.67). The EDX spectra of the ChAp samples did not show any pronounced peaks of Na and Cl (Fig. 3), what suggested that the synthesized apatite did not have substitutions in the cation (Na $\rightarrow$ Ca) and anion (Cl $\rightarrow$ OH) sublattices at the level detectable by the technique. In lyophilized materials a network of micrometer and submicrometer pores has been observed. The porous materials were produced by lyophilization of the samples immediately after rinsing and ageing. In the microscopic images of these materials two systems of pores can be visually distinguished (Fig. 4). Statistical treatment using the specialized computer programs "VideoTest 5.0" and "VideoSize 5.0" (St. Petersburg, Russia) has shown that the "small" pores have the average diameter of 30 μm, the "big" ones of 50 μm. Such pores could promote the bone tissue ingrowth into implanted material.

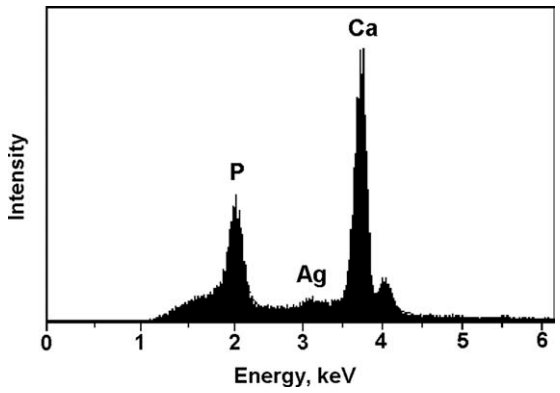


**FIGURE 3.** EDX spectrum of ChAp 50/50 composite. Ag signal is from the deposited thin conducting Ag film.

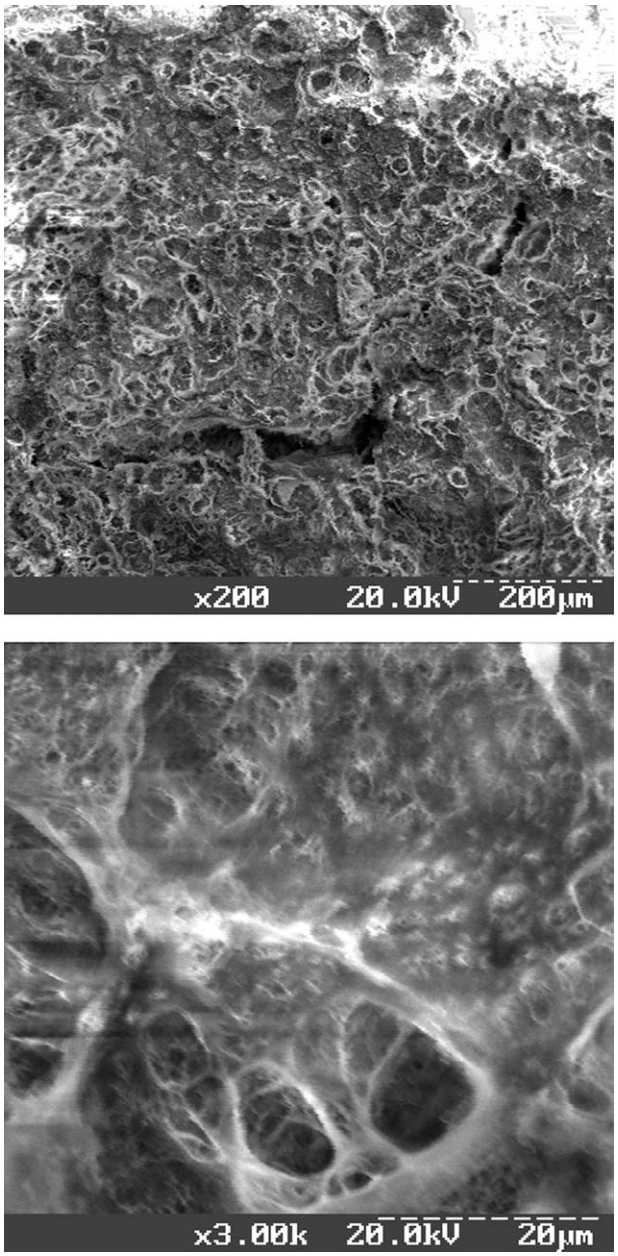


**FIGURE 4.** Microstructure of porous ChAp.

The content of Ca and P (measured by EDX microanalysis) in bones of the model animals after implantation of solid ChAp biomaterial with the 50/50 component ratio is shown in the Fig. 5. In this case it is clearly seen that in the presence of implanted ChAp, the Ca and P concentrations in bone tissue near the defect were restored much faster than in the control group (where the bone defects were not filled with implants).

The biochemical blood values for the experimental and control groups of animals are given in the Table III. The protein and alkaline phosphatase level in the blood of experimental animals do not differ from that of the control group. The comparison of the values with the results of microanalysis of bones with implanted ChAp indicates that calcium mobilization from the surface of intact tissues decreases while its content in blood plasma comes to normal. Low Ca mobilization from neighboring bones can decrease the bone strength loss accompanying the regenerative processes. As it is proved in numerous works [e.g., 37–40], the bone strength depends strongly on the mineral content, that is, Ca and P concentration.

These data suggest that nano-sized apatite crystals incorporated into chitosan matrix, being implanted *in vivo*, participate immediately in reparative biochemical processes of living bone tissue. Apparently, these are Ca and P from the apatite crystals of implanted material that are used for the regenerated bone formation. This decreases mobilization of these elements from the bone tissue near a defect.

The porous materials have shown osteoconductive properties in the *in vivo* tests. In five days after implantation, pores of ChAp were filled with the cells of leukocyte-macrophage and fibroblastic differons, which was the evidence of

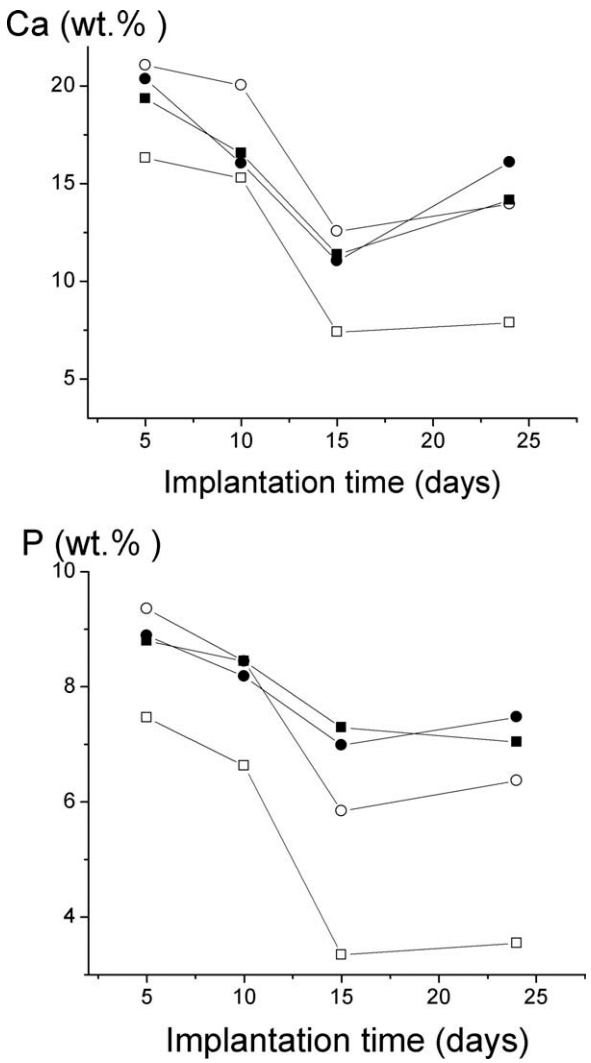


**FIGURE 5.** The content of Ca and P in bone tissue near the site of implantation (squares) and at the distance of 15 mm (circles) vs. implantation time. Non-filled symbols correspond to the control experiment: the defect without an implant.

**TABLE III. Biochemical Blood Values of the Experimental and Control Groups of Animals**

| | 10 days | | 15 days | | 24 days | |
|---|---|---|---|---|---|---|
| Value | Control | Experimental | Control | Experimental | Control | Experimental |
| Protein, g/L | 52.94 ± 1,78 | 64.05 ± 2.86 | 51.11 ± 2.04 | 60.35 ± 1.88 | 63.79 ± 2.41 | 61.22 ± 2.66 |
| Alkaline phosphatase, nmol/sL | 3116.91 ± 192.58 | 2401.63 ± 145.27 | 2334.01 ± 471.20 | 2774.02 ± 266.52 | 2343.42 ± 207.77 | 4236.53 ± 523.31 |
| Ca, mmol/L | 2.84 ± 0.33 | 2.06 ± 0.60 | 2.28 ± 0.14 | 1.48 ± 0.24 | 2.58 ± 0.27 | 2.05 ± 0.49 |

progress in osteoreparative process. Further, the formation of fibroreticular and membrane reticulated primary bone tissue trabecules occurred with their subsequent calcification and remodeling into lamellar bone tissue. Starting from the 10th day, the integration of ChAp into newly formed tissue was observed, and by the 24th day the replacement of the implant by the young bone took place. The above-described dynamics is specific only for porous samples of ChAp. Solid (nonporous) implants did not improve histological pattern of the reparative process.

The osteoconductive properties of a ChAp composite material can be observed after implantation of it into the bone defect at the first stages of regenerated bone tissue development. In the Figure 6 there are clearly visible pores filled with the typical for such regeneration stages cell and tissue species. Young granulation tissue (GT) dominates in the regenerate, its content is 25.25 ± 5.14%. We did not however observe the close connection of tissue components with the material of the implant, which can be explained by the early stage of observations and high rate of granulation tissue formation. GT occupies the peripheral segments of the defect (which is similar to the patterns of the control animals). The central pores of the implant are filled mostly with the cells of posttraumatic haematoma. The normal cell composition plays an important role in new bone formation. At the initial stage of regeneration the neutrophils secrete cytokines regulating proliferation, cell differentiation, and phagocytosis.[41] The lymphocytes and plasmocytes are able

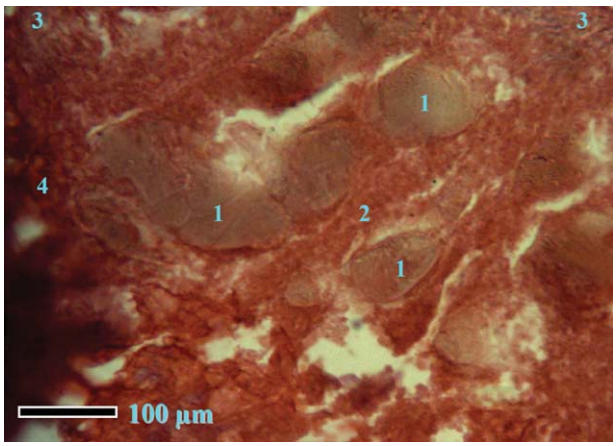


**FIGURE 6.** Area of the tibial defect, 5 days after traumatization: 1. ChAp. 2. Pore with posttraumatic haematoma cells. 3. Granulation tissue. 4. Capillary. [Color figure can be viewed in the online issue, which is available at wileyonlinelibrary.com.]

to regulate angiogenesis and fibroblast migration. Also they have stimulating influence on macrophages.[42] The macrophages in their turn act as regulators of inflammatory processes, they have chemotactic action on fibroblasts and provide intercellular cooperation in the focus of trauma.[43] Fibroblasts are the cells which actively produce collagen beginning from the first days after trauma providing the formation of a soft natural scaffold. So, proliferation and differentiation of cells at the first stage of the reparative regeneration is crucial for the formation of the critical mass of cells, which is important for the formation of tissue structures in trauma site at the following stages of regeneration.[44] In one field of view different cell phenotypes were observed: young secreting cells, mature macrophages filled with detritus, dying cells. The cell percentage for the experimental and control groups of animals are given in the Table IV. In the inner pores the edges of the material were blurred which could be indicative of the beginning of ChAp osteointegration and high activity of cells in this site of the defect. Both in the peripheral and in the central pores vascular invasion was observed, mostly of the sinusoidal type. The vessels were surrounded by a layer of perivascular cells and secreting fibroblasts, which were more numerous in peripheral sections.

In 10 days after introduction of the implant its intense biodegradation takes place with the formation of tissue-specific structures of regenerate. The intense growth of fibroreticular tissue (FT) with more ordered fiber arrangement can be observed in the area of the defect, and also formation of bone trabeculae of membrane reticulated bone begins (Fig. 7). FT is situated mostly along the periphery of the defect, while its central areas are filled with remains of granulation tissue with the great number of fibroblasts, macrophages, and sinusoidal capillaries. For the first time the formation of membrane reticulated bone tissue is observed which can be the evidence of the osteoblastic type of reparative processes. The amount

**TABLE IV. Cellular Composition of Regenerated Tissue in the Experimental and Control Groups of Animals, Five Days After Implantation**

| Cell type | Experimental group | Control group |
|---|---|---|
| Macrophages, % | 15.6 | 15.2 |
| Lymphocytes, % | 20.4 | 21.6 |
| Fibroblasts, % | 31.2 | 30.6 |
| Plasmocytes, % | 15.2 | 15.6 |
| Undifferentiated cells, % | 17.6 | 17.0 |

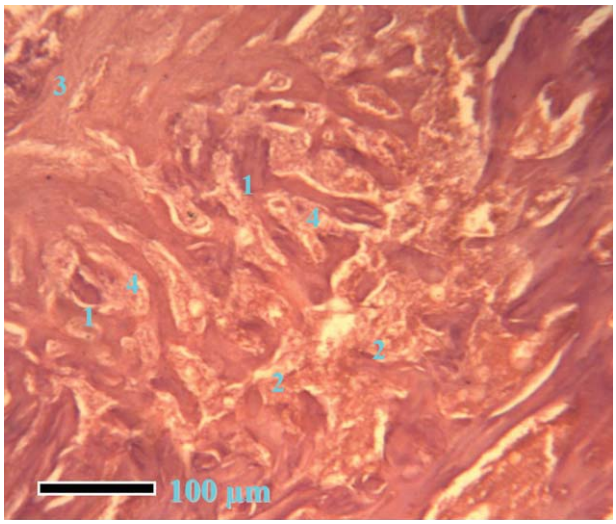


**FIGURE 7.** Area of the tibial defect, 10 days after traumatization: 1. ChAp. 2. Granulation tissue. 3. Fibroreticular tissue. 4. Bone trabeculae.

of new bone tissue is approximately the same as in the case of the control animals (34.58 ± 9.27%), so the implant cannot be regarded as osteoconductive. At the same time, the integration and close interconnection of the forming bone trabeculae and ChAp can be observed.

The histological pattern of the regenerate on the 15th day is similar to that of the 10th day (Fig. 8). Both fibroreticular and bone tissues were present; the bone tissue had formed a denser network of trabeculae than in the previous observation time. Granulation tissue was completely absent. The active remodeling of membrane reticulated bone into splenial bone and its mineralization takes place, which is indicated by the increase of staining intensity of the bone trabeculae. The percentage of FT, membrane reticulated bone and splenial bone is correspondingly 28.43 ± 7.97%, 40.21 ± 9.65%, and 10.87 ± 3.22%, which is in agreement

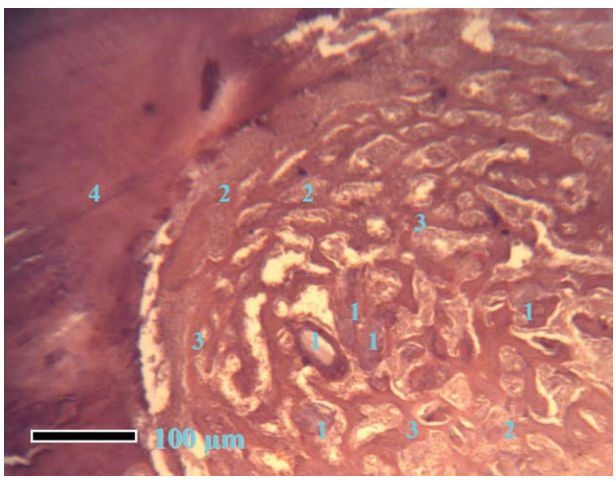


**FIGURE 8.** Area of the tibial defect, 15 days after traumatization: 1. ChAp. 2. Fibroreticular tissue. 3. Bone trabeculae. 4. "Parent" bone.

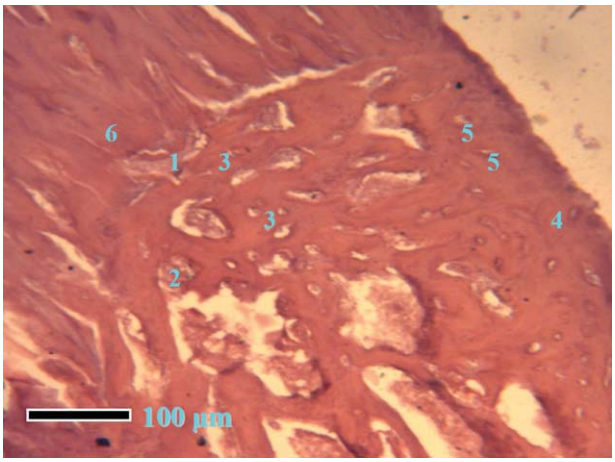


**FIGURE 9.** Area of the tibial defect, 24 days after traumatization: 1. ChAp. 2. Fibroreticular tissue. 3. Membrane reticulated bone tissue. 4. Splenial bone tissue. 5. Osteon. 6. "Parent" bone.

with the control series of animals. The remains of the implant are situated mainly in the centre of the defect, connected closely with the forming bone trabeculae and stained nonuniformly, which suggests their integration into the newly formed bone matrix.

On the 24th day of observation bone tissue occupies most of the area of the defect (Fig. 9). The deeper parts of the regenerate are formed with membrane reticulated bone tissue with stainability close to that of the "parent" bone. The number of osteoblasts on the surface of trabeculae decreases, which indicates that intense bone matrix formation processes stops, and remodeling processes begin. The remains of not degraded ChAp are pushed off to the periphery and are on the boundary of the "parent" bone. The tight bonding of the implant with newly formed bone matrix is observed; the bonding with the "parent" bone is less tight. The cortical plate in the place of the defect is formed mostly by the splenial bone in which intensive remodeling processes are observed, this is indicated by the presence of both secondary and primary osteons. The primary ones at this observation stage are much more numerous. So it is safe to say that the completion of the primary formation of neogenic bone and the beginning of remodeling processes. The implant's remains are closely integrated into the newly formed matrix and are subject to biodegradation in the course of bone remodeling.

## CONCLUSIONS

A series of chitosan/hydroxyapatite composite materials has been synthesized in aqueous medium from chitosan solution and soluble precursor salts by a one step coprecipitation method. XRD patterns of the materials suggest the presence of nanocrystalline apatite with the average crystallite size of ~20 nm. The similar size of crystallites is characteristic for natural bone bioapatite. The results of IR spectroscopy studies suggest the presence of carbonate ions in the synthesized materials. Thus, this relatively simple synthesis procedure

allows obtain composite materials with nanocrystalline carbonate-substituted hydroxyapatite similar to natural bone bioapatite. There are several works demonstrating the ability of chitosan-hydroxyapatite scaffolds to support bone cell attachment and growth using isolated cell cultures. But the behavior of scaffolds of such type in organisms, their biodegradation and replacement by bone tissue *in vivo* is much less studied. The objective of the present study was to examine *in vivo* behavior of simple chitosan/hydroxyapatite scaffolds placed into a perforated tibial defect of model laboratory animals following the main stages of reparative regeneration. In these experiments porous chitosan/hydroxyapatite materials have shown good osteoconductive properties. Histomorphological studies have shown that the porous chitosan/hydroxyapatite materials undergo almost complete biodegradation. The complete replacement of porous chitosan/hydroxyapatite composite implant by newly formed bone tissue within bone defects in rats takes place on the 24th day of implantation. The results of this study suggest the high potential of simple chitosan/hydroxyapatite composite scaffolds produced by the one-step co-precipitation method as a filling material for orthopaedy and stomatology.

## REFERENCES


1. Wahl DA, Czernuszka JT. Collagen-hydroxyapatite composites for hard tissue repair. Eur Cells Mater 2006;11:43–56.
2. Chang MC, Ko CC, Douglas WH. Preparation of hydroxyapatite-gelatin nanocomposite. Biomaterials 2003;24:2853–2862.
3. Yamaguchi I, Tokuchi K, Fukuzaki H, Koyama Y, Takakuda K, Monma H, Tanaka J. Preparation and microstructure analysis of chitosan/hydroxyapatite nanocomposites. J Biomed Mater Res 2001;55:20–27.
4. Rusu VM, Chuen-How Ng, Wilke M, Tiersch B, Fratzl P, Peter MG. Size-controlled hydroxyapatite nanoparticles as self-organized organic-inorganic composite materials. Biomaterials 2005;26: 5414–5426.
5. Hu Q, Li B, Wang M, Shen J. Preparation and characterization of biodegradable chitosan/hydroxyapatite nanocomposite rods via in situ hybridization: A potential material as internal fixation of bone fracture. Biomaterials 2004;25:779–785.
6. Elliott JC. Calcium phosphate biominerals. In: Kohn MJ, Rakovan J, Hughes JM, editors. Phosphates: Geochemical, Geobiological, and Materials Importance. Series: Reviews in mineralogy and geochemistry, vol. 48. Washington, DC: Mineralogical Society of America; 2002. p 427–454.
7. Zhang Y, Zhang MQ. Synthesis and characterization of macroporous chitosan/calcium phosphate composite scaffolds for tissue engineering. J Biomed Mater Res 2001;55:304–312.
8. Oliveira JM, Rodrigues MT, Silva SS, Malafaya PB, Gomes ME, Viegas CA, Dias IR, Azevedo JT, Mano JF, Reis RL. Novel hydroxyapatite/chitosan bilayered scaffold for osteochondral tissue-engineering applications: Scaffold design and its performance when seeded with goat bone marrow stromal cells. Biomaterials 2006;27:6123–6137.
9. Zhao F, Grayson WL, Ma T, Bunnell B, Lu WW. Effects of hydroxyapatite in 3-D chitosan-gelatin polymer network on human mesenchymal stem cell construct development. Biomaterials 2006;27:1859–1867.
10. Li J, Chen YP, Yin Y, Yao F, Yao K. Modulation of nano-hydroxyapatite size via formation on chitosan-gelatin network film in situ. Biomaterials 2007;28:781–790.
11. Wang L, Li C. Preparation and physicochemical properties of a novel hydroxyapatite/chitosan—Silk fibroin composite. Carbohydr Polym 2007;68:740–774.
12. Jiang LY, Lia YB, Zhanga L, Wang XJ. Preparation and characterization of a novel composite containing carboxymethyl cellulose used for bone repair. Mater Sci Eng C 2009;29:193–198.
13. Madhumathi K, Binulal NS, Nagahama H, Tamura H, Shalumon KT, Selvamurugan N, Nair SV, Jayakumar R. Preparation and characterization of novel β-chitin-hydroxyapatite composite membranes for tissue engineering applications. Int J Biol Macromol 2009;44:1–5.
14. Jiang L, Li Y, Wang X, Zhang L, Wen J, Gong M. Preparation and properties of nano-hydroxyapatite/chitosan/carboxymethyl cellulose composite scaffold. Carbohydr Polym 2008;74:680–684.
15. Li J, Dou Y, Yang J, Yin Y, Zhang H, Yao F, Wang V, Yao K. Surface characterization and biocompatibility of micro- and nano-hydroxyapatite/chitosan-gelatin network films. Mater Sci Eng C 2008;29:1207–1215.
16. Aimoli CG, Beppu MM. Precipitation of calcium phosphate and calcium carbonate induced over chitosan membranes: A quick method to evaluate the influence of polymeric matrices in heterogeneous calcification. Colloids Surfaces B Biointerfaces 2006;53: 15–22.
17. Muzzarelli RAA. Chitins and chitosans for the repair of wounded skin, nerve, cartilage and bone. Carbohydr Polym 2009;76:167–182.
18. Kong L, Gao Y, Lu G, Gong Y, Zhao N, Zhang X. A study on the bioactivity of chitosan/nano-hydroxyapatite composite scaffolds for bone tissue engineering. Eur Polym J 2006;42:3171–3179.
19. Leonor IB, Baran ET, Kawashita M, Reis RL, Kokubo T, Nakamura T. Growth of a bonelike apatite on chitosan microparticles after a calcium silicate treatment. Acta Biomaterialia 2008;4:1349–1359.
20. Manjubala I, Scheler S, Bossert J, Jandt KD. Mineralisation of chitosan scaffolds with nano-apatite formation by double diffusion technique. Acta Biomaterialia 2006;2:75–84.
21. Ito M. In vitro properties of a chitosan-bonded hydroxyapatite bone-filling paste. Biomaterials 1991;12:41–45.
22. Ge Z, Baguenard S, Lim LY, Wee A, Khor E. Hydroxyapatite-chitin materials as potential tissue engineered bone substitutes. Biomaterials 2004;25:1049–1058.
23. Balázsi C, Bishop A, Yang JHC, Balázsi K, Wéber F, Gouma PI. Biopolymer-hydroxyapatite scaffolds for advanced prosthetics. Compos Interfaces 2009;16:191–200.
24. Abdel-Fattah WI, Jiang T, El-Tabie El-Bassyouni G, Laurencin CT. Synthesis,characterization of chitosans and fabrication of sintered chitosan microsphere matrices for bone tissue engineering. Acta Biomaterialia 2007;3:503–514.
25. Chesnutt BM, Viano AM, Yuan Y, Yang Y, Guda T, Appleford MR, Ong JL, Haggard WO, Bumgardner JD. Design and characterization of a novel chitosan/nanocrystalline calcium phosphate composite scaffold for bone regeneration. J Biomed Mater Res A 2009;88:491–502.
26. Korzh NA, Dedukh NV. Reparative regeneration of bone: Modern view of the problem. Regeneration stages. Orthopaedy Traumatol Prosthetics (Ortopedia, travmatologia i protezirovanie) 2006;1: 77–83 (in Russian).
27. Wheater PR, Burkitt HG. Functional histology: A text and colour atlas, 2nd ed. Edinburgh and New York: Churchill Livingstone; 1987. p 348.
28. Fowler BO. Infrared studies of apatites. I. Vibrational assignments for calcium, strontium, and barium hydroxyapatites utilizing isotopic substitution. Inorg Chem 1974;13:194–207.
29. Markovic M, Fowler BO, Tung MS. Preparation and comprehensive characterization of a calcium hydroxyapatite reference material. J Res Natl Inst Stand Technol 2004;109:553–568.
30. Dyer JR. Applications of absorption spectroscopy of organic compounds. New Jersey: Prentice-Hall in Englewood Cliffs; 1965, 143 p.
31. Kumirska J, Czerwicka M, Kaczyński Z, Bychowska A, Brzozowski K, Thöming J, Stepnowski P. Application of spectroscopic methods for structural analysis of chitin and chitosan. Marine Drugs 2010;8:1567–1636.
32. Danilchenko SN, Koropov AV, Protsenko IYu, Sulkio-Cleff B, Sukhodub LF. Thermal behavior of biogenic apatite crystals in bone: An X-ray diffraction study. Cryst Res Technol 2006;41,3: 268–275.
33. Klug HP, Alexander LE. X-ray diffraction procedures for polycrystallite and amorphous materials, 2nd ed. New York: Wiley; 1974.
34. Danilchenko SN, Kukharenko OG, Moseke C, Protsenko IY, Sukhodub LF, Sulkio-Cleff B. Determination of the bone mineral crystallite size and lattice strain from diffraction line broadening. Cryst Res Technol 2002;37:1234–1240.

35. Eppell SJ, Tong W, Katz JL, Kuhn L, Glimcher MJ. Shape and size of isolated bone mineralites measured using atomic force microscopy. J Orthopaedic Res 2001;19:1027–1034.
36. Pramanik S, Agarwal AK, Rai KN. Trends Biomater Artif Organs 2005;19:46–53.
37. Tai K, Qi HJ, Ortiz C. Effect of mineral content on the nanoindentation properties and nanoscale deformation mechanisms of bovine cortical bone. J Mater Sci: Mater Med 2005;16:947–959.
38. Van der Linden JC, Birkenhäger-Frenkel DH, Verhaar JAN, Weinans H. Trabecular bone's mechanical properties and affected by its non-uniform mineral distribution. J Biomechan 2001;34:1573–1580.
39. Boivina G, Balaa Y, Doubliera A, Farlay D, Ste-Marie LG, Meunier PJ, Delmas PD. The role of mineralization and organic matrix in the microhardness of bone tissue from controls and osteoporotic patients. Bone 2008;43:532–538.
40. Cowin SC, ed. Bone Mechanics Handbook. Boca Raton, FL: CRC Press; 2001. 981 p. (ISBN: 0849391172).
41. Cancedda R, Quarto R, Giannoni P, et al. Cell therapy and bone repair. Eur Cells Mater 2003;5(Suppl 2): 2–3.
42. Kaspar D, Neidlinger-Wilke C, Holbein O. Mitogens are increased in the systemic circulation during bone callus healing. J Orthop Res 2003;21:320–325.
43. Ross FP. Cytokine regulation of osteoclast formation and function. J Musculoskel Neuron Interact 2003;3:282–286.
44. Grundnes O, Reikeras O. The importance of the hematoma for fracture healing in rats. Acta Orthop Scand 1993;64:340–342.